Stabilizing photoassociated Cs_2 molecules by optimal control*

Zhang Wei(张 为), Xie Ting(谢 廷), Huang Yin(黄 寅), Wang Gao-Ren(王高仁), and Cong Shu-Lin(丛书林)†

School of Physics and Optoelectronic Technology, Dalian University of Technology, Dalian 116024, *China*

(Received 13 April 2012; revised manuscript received 23 June 2012)

We demonstrate theoretically that photoassociated molecules can be stabilized to deeply bound states. This process is achieved by transferring the population from the outer well to the inner well using the optimal control theory, the Cs_2 molecule is taken as an example. Numerical calculations show that weakly bound molecules formed in the outer well by a pump pulse can be compressed to the inner well via a vibrational level of the ground electronic state as an intermediary by an additionally optimized laser pulse. The positively chirped pulse can enhance the population of the target state. With a transform-limited dump pulse, nearly all the photoassociated molecules in the inner well of the excited electronic state can be transferred to the deeply vibrational level of the ground electronic state.

Keywords: ultracold molecule, photoassociation, optimal control

PACS: 33.80.–b, 32.80.Qk **DOI:** 10.1088/1674-1056/22/1/013301

1. Introduction

Photoassociation (PA) has captured much attention from researchers due to its wide applications in forming ultracold molecules and reaching ultralow temperatures.[1–7] In most experimental situations, photoassociated molecules are prepared in the higher vibrational states of an excited electronic state, and these unstable molecules may become free atoms again owing to subsequent collisions. In order to prepare stable molecules, the weakly bound molecules in the excited electronic state must be transferred to the ground or the lowest-triplet state. In the special case of the excited potential of the Cs_2 molecule with a double well $0_g^-(6s+6p_{3/2})$, the smooth barrier between the two wells acts as a speed bump and slows down the vibrational motion in the outer well so that the vertical transitions can take place at an intermediate distance $R_{\rm int}$. A dump pulse can be used to transfer the population from the excited electronic state to the ground electronic state when the wave packets move to the vicinity of the barrier.[1]

However, the wave packets in the outer well of the excited electronic state have small Franck–Condon (FC) factors with the lower vibrational states of the ground electronic state, and less of the population will be transferred to form stable molecules in the ground electronic state. A small number of wave packets can pass through the barrier via a tunneling effect and move to the smaller internuclear distance. Hence, a question is put forward, how can we populate the lower vibrational states to stabilize the photoassociated molecules.

With the development of laser techniques,[8,9] shaping technologies of laser pulses have been applied to the investigation of the PA reaction,[10–15] which paves the way for implementing the optimal control of atoms and molecules by using ultrashort pulse lasers. The optimal control theory (OCT)[16] offers the prospect of using an external field to drive atoms or molecules to a desired state. In theory, the algorithms for OCT have been developed,[17–23] and applied widely to many research fields.[24–27] Experimentally, the optimal control has been realized using a feedback learning loop.[28] The formations of ultracold molecules, specifically the optimal conversion of atoms into a molecular Bose–Einstein condensation,[29] have been investigated by OCT. Here, we start from weakly bound Cs_2 molecules formed in the outer well with a pump pulse. An additional optimized shaped pulse, whose spectral width is enough to cover the energy difference between the initial state and an eigenstate in the inner well, is then used to transfer the population from the outer well to the inner well via a vibrational state of the ground electronic state by employing the OCT. Most of the population can be transferred from the outer well into the inner well. Finally, with a transform-limited dump pulse, nearly all the molecules in the inner well of the excited electronic state can be stabilized in the lower vibrational state of the ground electronic state.

2. Theoretical approach

2.1. The Cs_2 system

Our investigation starts with a two-state Cs_2 model, which can be described by the time-dependent Schrödinger equation (TDSE)

$$\begin{aligned} & i\hbar\frac{\partial}{\partial t}\begin{pmatrix}\Psi_g(R,t)\\ \Psi_e(R,t)\end{pmatrix} \\ &= \begin{pmatrix}\hat{T}+V_g(R)+\frac{1}{2}\hbar\omega_L(t) & \hat{W}(t)\\ \hat{W}(t) & \hat{T}+V_e(R)-\frac{1}{2}\hbar\omega_L(t)\end{pmatrix} \\ &\times\begin{pmatrix}\Psi_g(R,t)\\ \Psi_e(R,t)\end{pmatrix}, \end{aligned} \tag{1}$$

where $\Psi_g(R,t)$ and $\Psi_e(R,t)$ denote the wave functions of the $a^3\Sigma_u^+$ and 0_g^- states, respectively, $\hat{T}$ is the kinetic-energy op-

*Project supported by the National Natural Science Foundation of China (Grant No. 10974024) and the SRFDP, China (Grant No. 20090041110025).

†Corresponding author. E-mail: shlcong@dlut.edu.cn

© 2013 Chinese Physical Society and IOP Publishing Ltd

erator, and $\omega_L(t)$ is the carrier-frequency of the laser pulse, which is time-dependent if the chirping effect is considered. The rotating-wave approximation (RWA) is employed here. The interaction $\hat{W}(t)$ is written as

$$\hat{W}(t) = -\frac{1}{2}\varepsilon(t)\hat{e}_L \cdot \hat{\mu}, \tag{2}$$

where $\hat{\mu}$ is the dipole moment operator, $\hat{e}_L$ is the polarization vector of the electric field, and $\varepsilon(t) = \varepsilon_0 f(t)$ is the electric field with peak amplitude ε_0 and envelope $f(t)$ without an oscillating term. In the calculations, we use a constant dipole moment $\mu = 3.64$ a.u.,[30] since the R-dependent dipole moment was not found in the literature. Thus, the interaction $\hat{W}(t)$ can be rewritten as

$$\hat{W}(t) = -W_0 f(t), \tag{3}$$

where $W_0 = \varepsilon_0 \mu/2$.

As shown in Fig. 1, the $0_g^-(6s_{1/2}+6p_{3/2})$ potential has a double-well structure with a barrier situated at approximately $15a_0$. Only the levels in the outer well have relatively large Franck–Condon factors with the scattering state. Hence, the photoassociated molecules produced by the pump pulse are mainly bound in the outer well. In this paper, we consider the renormalized wave function of the 0_g^- state after the pump pulse as the initial state, which is a superposition of the relevant vibrational eigenstates. We utilize an additional optimized pulse, whose spectral width covers the energy difference between a vibrational eigenstate (target state) in the inner well and all vibrational eigenstates of the initial state, to transfer most of the probability density (or population) to the inner well via a higher vibrational state of the $a^2\Sigma_u^+$ state. Thus, nearly all of the population in the inner well can be transferred to a lower vibrational state of the $a^2\Sigma_u^+$ state by a transform-limited Gaussian pulse.

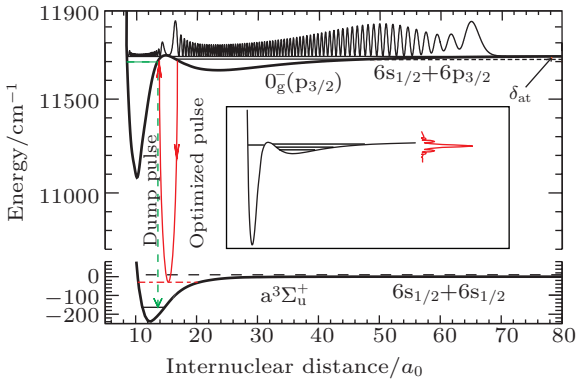


Fig. 1. (color online) The potential curves of the ground triplet state $a^3\Sigma_u^+$ and the excited state 0_g^- of the cesium dimer. The photoassociated molecules can be compressed to the inner well by an optimal pulse and finally dumped to a deeply bound vibrational state of the $a^3\Sigma_u^+$ state by a transform-limited pulse. The dashed line directly above the $a^3\Sigma_u^+$ state denotes the initial continuum level, and δ_{at} represents the detuning deviating from the D_2 atomic resonance line. The short-range potential curves taken from Ref. [39] are matched to long-range dispersion potentials with C_n coefficients.[40] In the inset, the red line denotes the spectrum of an optimized laser pulse, solid lines in the outer well show the eigenenergies superposing the initial state, and the solid line in the inner well indicates the target state.

2.2. Brief review of optimal control theory

An external field is utilized to drive a system from an initial state $|\phi_i\rangle$ to a specified target state $|\phi_f\rangle$. The formal solution of the wave function at time t is given by

$$|\phi(t)\rangle = \hat{U}(t,0)|\phi_i\rangle, \tag{4}$$

where $\hat{U}(t,0)$ denotes the evolution operator. In order to obtain an optimal field, an objective function F is defined as

$$F = |\langle\phi_i|\hat{U}^+(T,0;\varepsilon)|\phi_f\rangle|^2. \tag{5}$$

The field is optimized when F is close to 1.0.

The F is a function of field $\varepsilon(t)$ and depends on the final time T. In order to use the dynamical information from intermediate time, we define a new functional J

$$J = -F + \int_0^T g(\varepsilon)\,\mathrm{d}t, \tag{6}$$

where $g(\varepsilon)$ denotes an additional constraint over the field. The optimal field can be obtained by minimizing J based on the replacement rule in the control equation for the field. However, the choice of $g(\varepsilon)$ can not be arbitrary, since it may lead to a vanishing change in the field as the optimum is realized, and it needs to satisfy the requirements of monotonic convergence.[17] In the present work, $g(\varepsilon)$ is chosen to be

$$g(\varepsilon) = \frac{\lambda}{S(t)}[\varepsilon(t) - \tilde{\varepsilon}(t)]^2, \tag{7}$$

where $\tilde{\varepsilon}(t)$ is the field in the previous iteration and corresponds to a minimal change in the pulse energy at that iteration. The $S(t)$ denotes the shape function, which is the constraint used to switch the field smoothly on and off. We choose it to be $S(t) = \sin^2(\pi t/T)$. The optimization strategy can be controlled by the parameter λ. A small value results in a small weight of the additional constraint and allows for a large modification in the field, while a large value of λ represents a conservative search strategy with only a small modification in the field at each iteration.[31,32]

We employ the Krotov algorithm[17,33–35] to obtain the control equations. The derivation of the algorithm for the objective function (Eq. (5)) and the constraint (Eq. (7)) can be found in Ref. [31]. But in the rotating-wave approximation, the theoretical treatment of the optimization strategy is somewhat different from that in Ref. [31]. In the present work, we only deal with the amplitude shaping not the phase shaping. Thus, we need to use a trick[36–38] to ensure that the envelope is always positive. We do this by using a mathematical control parameter $u(t) = \sqrt{\varepsilon(t)}$, and $S'(t) = \sqrt{S(t)}$. Then, we

derive the control equations for $u(t)$ at the k-th iteration step as follows (see Appendix A for the derivation):

$$u_{k+1}(t) = u_k(t) + 2u_k(t)\frac{S'(t)}{\lambda}\,\mathrm{Im}\{\langle\phi_\mathrm{i}|\hat{U}^+(T,0;\varepsilon_k)|\phi_\mathrm{f}\rangle \times \langle\phi_\mathrm{f}|\hat{U}^+(t,T;\varepsilon_k)\hat{\mu}\hat{U}(t,0;\varepsilon_{k+1})|\phi_\mathrm{i}\rangle\}, \quad (8)$$

$$\varepsilon_{k+1}(t) = u^2_{k+1}(t), \quad (9)$$

where $\varepsilon(t)$ is solved by employing two different grids in the time discretization (see Ref. [31] for details).

3. Results and discussion

In our calculation, the short-range potential curves taken from Ref. [40] are matched to long-range dispersion potentials with C_n coefficients.[40] The initial wave function is calculated by diagonalizing the Hamiltonian in Eq. (1) on a mapped Fourier grid in the absence of the laser field.[41,42] The dynamics process is described by numerically solving the TDSE using the Chebyshev propagator.[43]

The numerical computations are performed within the framework of size $L_\mathrm{R} = 19250a_0$. A new initial state is taken to be the renormalized wave packet at the 0^-_g state created by the pump pulse at temperature $T = 54$ μK. In this paper, the target state is chosen to be an eigenstate $v = 106$ mainly bound in the inner well. We consider two cases, in whcih the initial wave packets are excited by pump-1 and pump-2 pulses, respectively. The peak intensity of the pump-2 pulse is larger than that of the pump-1 pulse.

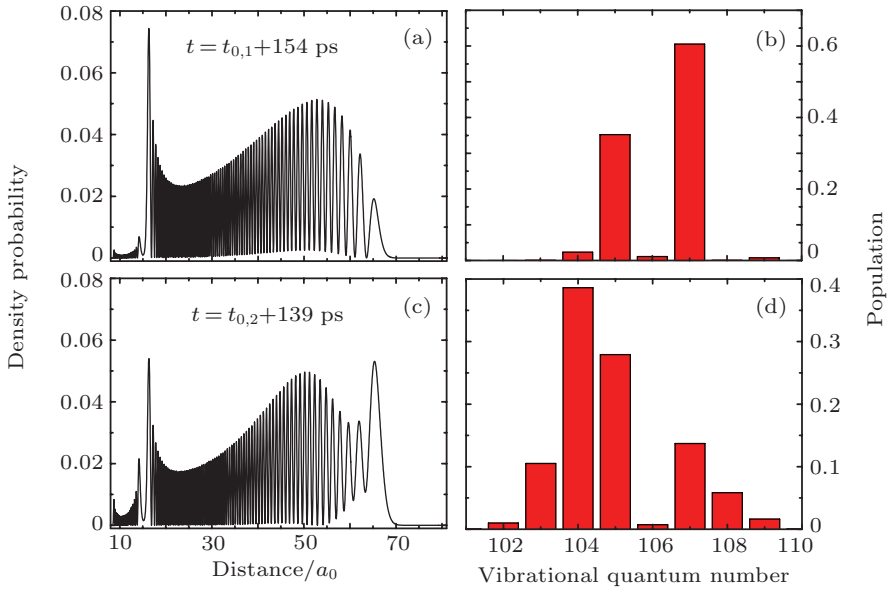


Fig. 2. (color online) (a) and (c) Probability density versus internuclear distance, and (b) and (d) population versus vibrational quantum number. Two cases are considered. In panels (a) and (b), the initial wave packet is excited by the pump-1 pulse with peak intensity $E_{0,1} = 0.28$ MV/m, full width at half maximum $\tau_1 = 40$ ps, central time $t_{0,1} = -100$ ps, and red detuning $\delta_{\mathrm{at},1} = 7.6$ cm^{-1} at $t = t_{0,1}$+154 ps. In panels (c) and (d), the initial wave packet is excited by the pump-2 pulse with $E_{0,2} = 0.71$ MV/m, $\tau_2 = 40$ ps, $t_{0,2} = -100$ ps, and $\delta_{\mathrm{at},2} = 7.6$ cm^{-1} at $t = t_{0,2}$+139 ps.

Figure 2(a) shows the initial state $\phi_{\mathrm{i},1}$ created by pump-1 at $t = t_{0,1} + 154$ ps. The parameters of the pump-1 pulse are chosen to be peak intensity $E_{0,1} = 0.28$ MV/m, full width at half maximum $\tau_1 = 40$ ps, central time $t_{0,1} = -100$ ps, and red detuning $\delta_{\mathrm{at},1} = 7.6$ cm^{-1}. The corresponding population distribution at the 0^-_g state is illustrated in Fig. 2(b), from which we see that the photoassociated molecules mainly distribute on the vibrational levels $v = 105$ and 107, and only a small part is on the $v = 104$, 106, and 109 levels. Figure 2(c) displays the initial state $\phi_{\mathrm{i},2}$ created by the pump-2 pulse at $t = t_{0,2} + 139$ ps. The parameters of the pump-2 pulse are taken to be the same as those of the pump-1 pulse except for the peak intensity $E_{0,2} = 0.71$ MV/m. The population distribution on the relevant vibrational levels is shown in Fig. 2(d).

In the two cases, two initial guess fields (guess-1 field and guess-2 field) corresponding to the two initial states $\phi_{\mathrm{i},1}$ and $\phi_{\mathrm{i},2}$ are treated separately, which are shown by the red-dashed lines in Figs. 4(a) and 4(c). For the guess-1 field, the parameters are taken to be peak amplitude $E_{0,1} = 11.3$ MV/m, full width at half maximum $\tau_1 = 60$ ps, central time $t_{0,1} = 150$ ps, and carrier frequency $\omega_{\mathrm{L},1} = 11799.3$ cm^{-1}. The parameters of the guess-2 field are the same as those of the guess-1 field except $\omega_{\mathrm{L},2} = 11799.0$ cm^{-1}. The time scale for the optimal control is restricted to 300 ps, and the initial time is taken to be 0. The populations at the target state (objective function F) versus the iteration number are shown in Fig. 3. For the initial state $\phi_{\mathrm{i},1}$, F is equal to 0.982 after 110 iterations. And for the initial state $\phi_{\mathrm{i},2}$, which is a coherent superposition of more vibrational eigenstates, $F = 0.931$ after 97 iterations.

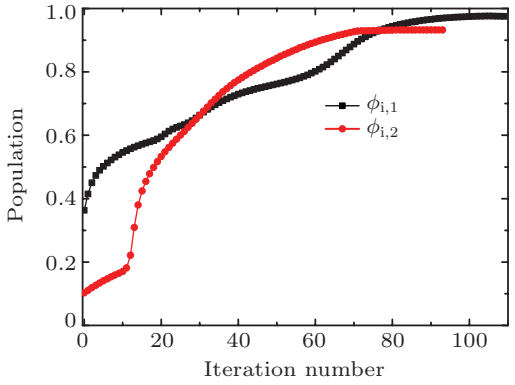


Fig. 3. (color online) The population of target state versus iteration number in guess-1 field with peak amplitude $E_{0,1} = 11.3$ MV/m, full width at half maximum $\tau_1 = 60$ ps, central time $t_{0,1} = 150$ ps, and carrier frequency $\omega_{L,1} = 11799.3$ cm^{-1} and guess-2 field with the same parameters as those in guess-1 except $\omega_{L,2} = 11799.0$ cm^{-1}.

The envelopes of the two guess fields and the optimal laser pulses are plotted in Figs. 4(a) and 4(c), and the corresponding spectra in the frequency domain are shown in Figs. 4(b) and 4(d). The optimized pulses differ from the guess fields. Many oscillating patterns appear in Figs. 4(a) and 4(c). The insets in Fig. 4 illustrate the shapes of the envelopes within a time scale of 1 ps: they are still smooth enough, and in such a time scale, there are more than 353.7 optical cycles. In Fig. 4(b), the most intense peak emerges at 11799.3 cm^{-1} corresponding to the central frequency of the guess field. There are several hypo-peaks appearing in the frequency spectrum because the initial state includes the components of a few vibrational eigenstates. Compared with Fig. 4(b), figure 4(d) displays more hypo-peaks because more vibrational eigenstates are included in the initial state. However, both frequency spectra display symmetric structures.

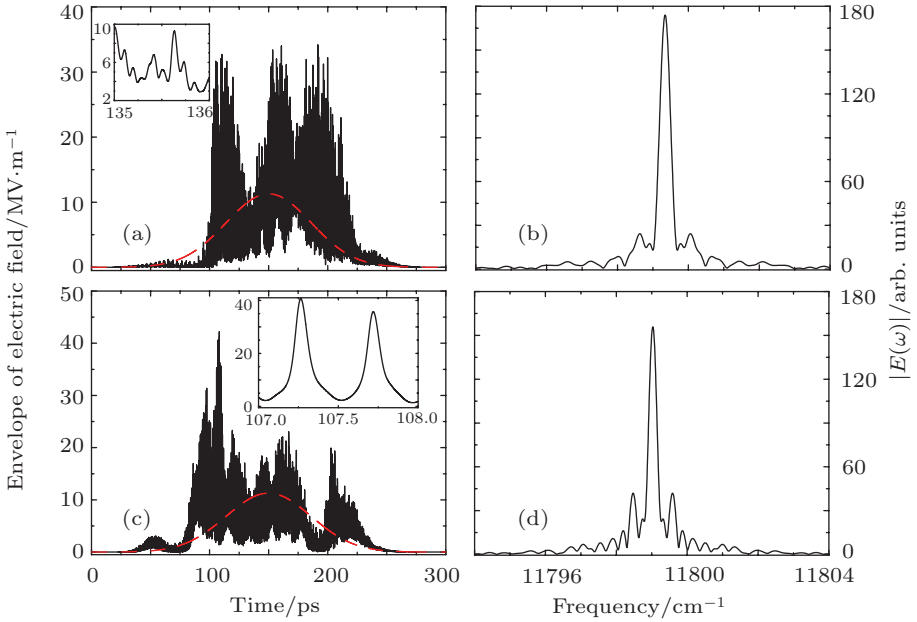


Fig. 4. (color online) (a) The temporal envelopes of the guess-1 field (red-dashed line) and its corresponding optimal field (black-solid line), (b) the spectrum of the optimal field in panel (a), (c) the temporal envelopes of the guess-2 field (red-dashed line) and its corresponding optimal field (black-solid line), (d) the spectrum of the optimal field in panel (c). The insets illustrate the shapes of the envelopes within a time scale of 1 ps.

To better understand the optimal control process, the time-dependent expectations

$$\langle R\rangle(t) = \langle \Psi_e(t)|R|\Psi_e(t)\rangle / |\Psi_e(t)|^2$$

of internuclear distance in the 0_g^- state are plotted in Fig. 5. When $\phi_{i,1}$ is taken to be the initial state, $\langle R\rangle(t)$ increases with increasing time before $t = 50$ ps (black line), because the wave packet is moving outward in the outer well after it has been reflected by the barrier. The population of the 0_g^- state (not shown) begins to be transferred to the ground electronic state when $t = 50$ ps. Most of population transferred to the ground electronic state returns back to the 0_g^- state when the pulse ends, but is bound on the level $v = 106$ in the inner well. The $\langle R\rangle(t)$ is approximately equal to $12.8a_0$, which shows that the wave packet (or the probability density) distributes in a small range of internuclear distance. When the initial state is $\phi_{i,2}$, $\langle R\rangle(t)$ increases before 70 ps with the increasing time (red line), and decreases afterwards. When the optimized pulse is over, the population is transferred to the inner well, and

$$\langle R\rangle(t = 300 \text{ ps}) = 13.1a_0.$$

We now discuss the positive chirping effect of the guess field on the optimal control process. The envelope of the optimal guess field is expressed as[30]

$$\varepsilon(t) = \frac{\varepsilon_0}{\sqrt{1+(\chi\tau^2)^2/(4\ln 2)^2}} \exp\left[-2\ln 2\left(\frac{t-t_0}{\tau}\right)^2\right]. \quad (10)$$

The parameters of the guess field are chosen to be the same as those of guess-2 except for the chirped rate $\chi = 1.012 \times 10^{-12}$ a.u., which ensures the scanning range to cover the energy difference between the highest and the lowest vibrational levels in the initial state $\phi_{i,2}$. The population of the target state is 0.958 after 120 iterations as shown in Fig. 6(a), which is larger than the result (0.931) in Fig. 3. The guess field and the optimized field are shown in Fig. 6(b). Generally, the intensity of the optimized field is lower than that in Fig. 4(c). The time- and frequency-resolved spectrum of the optimal pulse is shown in Fig. 6(c). The most intense peak in the frequency domain appears at 11797.2 cm^{-1}, and three apparent hypo-peaks emerge at 11797.9 cm^{-1}, 11798.8 cm^{-1}, and 11799.6 cm^{-1} respectively. The shape of the spectrum in the time domain also displays an oscillating pattern. Since the wave packet is reflected outward by the barrier, $\langle R\rangle(t)$ increases before $t = 70$ ps, and then decreases gradually, as shown in Fig. 6(d). Finally, $\langle R\rangle(t) = 12.78a_0$ when the laser pulse is over. We also calculate the dynamic process with negatively chirped pulses, the result shows no advantages, so we do not present it.

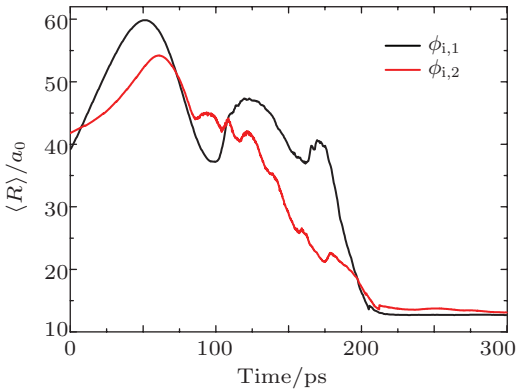


Fig. 5. (color online) The expectation $\langle R\rangle$ in the 0_g^- state versus time under the action of optimal pulses shown in Figs. 4(a) and 4(c).

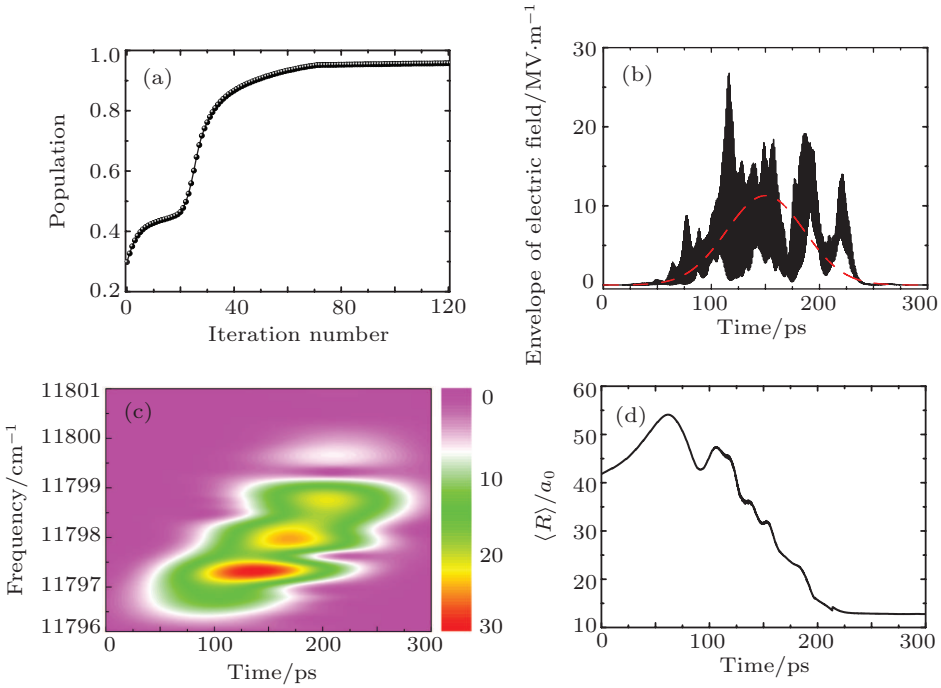


Fig. 6. (color online) (a) The population of the target state versus iteration number, (b) temporal envelope of the guess field (red-dashed line) and its corresponding optimal field, (c) the time- and frequency-resolved spectrum of the optimal laser field, (d) the expectation $\langle R\rangle$ in the 0_g^- state versus time. The guess field parameters are the same as those of the guess-2 field except for the chirped rate $\chi = 1.012 \times 10^{-12}$ a.u.

Table 1. Parameters for the dump pulses: peak amplitude $E_{0,i}$ of the electric field, full width at half maximum τ_i, central time $t_{0,i}$, the carrier frequency ω_L, and transfer efficiency.

v'	$E_{0,i}$/MV·m^{-1}	τ_i/ps	t_0/ps	ω_L/cm^{-1}	Efficiency
10	0.38	35.36	375	11872.34	0.990
9	0.44	60.1	500	11881.59	0.991

When the wave packet is compressed into the inner well, it is bound in the vibrational state $v = 106$. We can utilize a transform-limited pulse to dump the population from the $v = 106$ level to the vibrational levels $v' = 10$ and 9 of the ground electronic state. The dump pulse parameters and the transfer efficiencies on the $v' = 9$ and 10 levels are shown in Table 1. The corresponding time-dependent populations are displayed in Fig. 7. The populations of the target states increase steadily, yielding very high values at the ends of the pulses. The transfer efficiencies shown in Table 1 are better than those in Ref. [1] where only the population of 0.12 on the $v' = 14$ level was obtained.

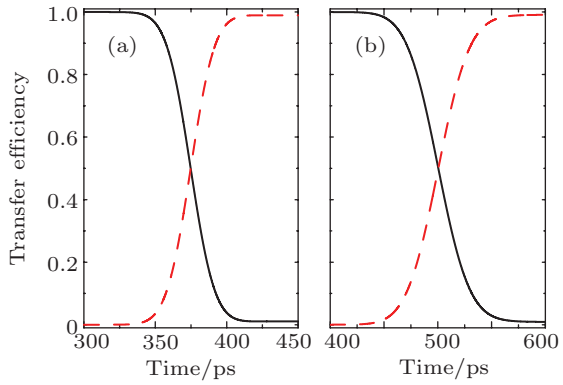


Fig. 7. (color online) (a) The time-dependent population of $v = 106$ (black-solid line) and $v' = 10$ (red-dashed line) with the laser pulse in the first row of Table 1. (b) The time-dependent population of $v = 106$ (black-solid line) and $v' = 9$ (red-dashed line) with the laser pulse in the second row of Table 1.

4. Conclusion

We investigate theoretically how to stabilize photoassociated molecules to deeply bound states by transferring the population from the outer well to the inner well using the optimal control theory and take the Cs_2 molecule as an example. Numerical calculations show that weakly bound molecules formed in the outer well by a pump pulse can be transferred to the inner well via the vibrational state of the ground electronic state as an intermediary by utilizing an additional optimized shaped pulse whose spectral width is enough to cover the energy difference between the initial state and the target state in the inner well. The population of the target state can be enhanced by the positive chirped pulse. Nearly all molecules in the inner well of the excited electronic state can be transferred to the lower vibrational level $v' = 10$ or 9 of the ground electronic state by a transform-limited dump pulse.

Appendix A: OCT in RWA

The Hamiltonian can be written as

$$H = H_0 + \varepsilon(t)\mu, \tag{A1}$$

where H_0 denotes the Hamiltonian in the absence of a laser field. Let $\varepsilon(t) = u(t)^2$, then the control equation can be expressed as[17,31]

$$\varepsilon_{k+1}(t) = \varepsilon_k(t) + \frac{S(t)}{\lambda}\,\mathrm{Im}\left\{\langle\phi_\mathrm{i}|\hat{U}^+(T,0;\varepsilon_k)|\phi_\mathrm{f}\rangle \times \langle\phi_\mathrm{f}|\hat{U}^+(t,T;\varepsilon_k)\left|\frac{\partial\hat{H}}{\partial\varepsilon}\right|_{\varepsilon_{k+1}}|\hat{U}(t,0;\varepsilon_{k+1})|\phi_\mathrm{i}\rangle\right\}. \tag{A2}$$

We use $u(t)$ as the control parameter instead of $\varepsilon(t)$. Using $\frac{\partial\hat{H}}{\partial u} = \frac{\partial\hat{H}}{\partial\varepsilon}\cdot\frac{\partial\varepsilon}{\partial u}$ and $S'(t) = \sqrt{S(t)}$, we get a new control equation

$$u_{k+1}(t) = u_k(t) + 2u_{k+1}(t)\frac{S'(t)}{\lambda}\,\mathrm{Im}\{\langle\phi_\mathrm{i}|\hat{U}^+(T,0;\varepsilon_k)|\phi_\mathrm{f}\rangle \times \langle\phi_\mathrm{f}|\hat{U}^+(t,T;\varepsilon_k)\hat{\mu}\hat{U}(t,0;\varepsilon_{k+1})|\phi_\mathrm{i}\rangle\}. \tag{A3}$$

The $2u_{k+1}(t)$ on the right-hand side can be approximated as $2u_k(t)$, and the control equation can be rewritten as

$$u_{k+1}(t) = u_k(t) + 2u_k(t)\frac{S'(t)}{\lambda}\,\mathrm{Im}\{\langle\phi_\mathrm{i}|\hat{U}^+(T,0;\varepsilon_k)|\phi_\mathrm{f}\rangle \times \langle\phi_\mathrm{f}|\hat{U}^+(t,T;\varepsilon_k)\hat{\mu}\hat{U}(t,0;\varepsilon_{k+1})|\phi_\mathrm{i}\rangle\}. \tag{A4}$$

References

[1] Koch C P, Luc-Koenig E and Masnou-Seeuws F 2006 *Phys. Rev.* A **73** 033408
[2] Koch C P, Kosloff R and Masnou-Seeuws F 2006 *Phys. Rev.* A **73** 043409
[3] Koch C P, Kosloff R, Luc-Koenig E, Masnou-Seeuws F and Crubellier A 2006 *J. Phys.* B **39** S1017
[4] Shapiro E A, Shapiro M, Pe'er A and Ye J 2007 *Phys. Rev.* A **75** 013405
[5] Poschinger U, Salzmann W, Wester R, Weidemüller M, Koch C P and Kosloff R 2006 *J. Phys.* B **39** S1001
[6] Liu L, Niu Y Y, Yuan K J and Cong S L 2007 *Chin. Phys.* **16** 2957
[7] Zhang H S, Ji Z H, Yuan J P, Zhao Y T, Ma J, Wang L R, Xiao L T and Jia S T 2011 *Chin. Phys.* B **20** 123702
[8] Ran L L, Qu S L and Guo Z Y 2010 *Chin. Phys.* B **19** 034204
[9] Zhou Y, Miao Q and Wang C K 2011 *Chin. Phys.* B **20** 044205
[10] Mullins T, Salzmann W, Götz S, Albert M, Eng J, Wester R and Weidemüller M. 2009 *Phys. Rev.* A **80** 063416
[11] Merli A, Eimer F, Weise F and Lindinger A 2009 *Phys. Rev.* A **80** 063417
[12] Zhang W, Huang Y, Xie T, Wang G R and Cong S L 2010 *Phys. Rev.* A **82** 063411
[13] Zhang W, Wang G R and Cong S L 2011 *Phys. Rev.* A **83** 045401
[14] Zhang W, Xie T, Huang Y and Cong S L 2011 *Phys. Rev.* A **84** 065406
[15] Zhang W, Zhao Z Y, Xie T, Wang G R, Huang Y and Cong S L 2011 *Phys. Rev.* A **84** 053418
[16] Rice S A and Zhao M 2000 *Optimal Control of Molecular Dyanmics* (New York: Wiley)
[17] Palao J P and Kosloff R 2003 *Phys. Rev.* A **68** 062308
[18] Rabitz H, Hsieh M and Rosenthal C 2004 *Science* **303** 1998
[19] Zhu W and Rabtiz H 1998 *J. Chem. Phys.* **109** 385
[20] Zhu W and Rabitz H 1999 *J. Chem. Phys.* **110** 7142
[21] Ho T S and Rabitz 2010 *Phys. Rev.* E **82** 026703
[22] Liao S T, Ho T S, Chu Shih-I and Rabitz H 2011 *Phys. Rev.* A **84** 031401(R)
[23] Schirmer S G and de Fouquieres P 2011 *New J. Phys.* **13** 073029
[24] Müller M M, Reich D M, Murphy M, Yuan H, Vala J, Whaley K B, Calarco T and Koch C P 2011 *Phys. Rev.* A **84** 042315
[25] Kurosaki Y, Yokoyama K and Yokoyama A 2009 *J. Chem. Phys.* **131** 144305
[26] Mishima K and Yamashita K 2009 *J. Chem. Phys.* **131** 014109
[27] de Lima E F, Ho T S and Rabitz H 2011 *Chem. Phys. Lett.* **501** 267
[28] Brixner T and Gerber G 2003 *Chem. Phys. Chem.* **4** 418
[29] Hornung T, Gordienko S, de Vivie-Riedle R and Verhaar B J 2002 *Phys. Rev.* A **66** 043607
[30] Luc-Koenig E, Kosloff R, Masnou-Seeuws F and Vatasescu M 2004 *Phys. Rev.* A **70** 033414
[31] Koch C P, Palao J P, Kosloff R and Masnou-Seeuws F 2004 *Phys. Rev.* A **70** 013402
[32] Ndong M and Koch C P 2010 *Phys. Rev.* A **82** 043437
[33] Krotov V F 2008 *Dokl. Math.* **78** 949
[34] Krotov V F 2009 *Autom. Remote Control* **70** 357
[35] Sklarz S E and Tannor D J 2002 *Phys. Rev.* A **66** 053619
[36] Ohtsuki Y and Nakagami K 2008 *Phys. Rev.* A **77** 033414
[37] Lapert M, Tehini R, Turinici G and Sugny D 2008 *Phys. Rev.* A **78** 023408
[38] Ho T S, Rabitz H and Chu Shih I 2011 *Com. Phys. Comm.* **182** 14
[39] Comparat D, Drag C, Tolra B L, Fioretti A, Pilleta P, Crubellier A, Dulieu O and Masnou-Seeuws F 2000 *Eur. Phys. J.* D **11** 59
[40] Vala J, Dulieu O, Masnou-Seeuws F, Pillet P and Kosloff R 2000 *Phys. Rev.* A **63** 013412
[41] Kokoouline V, Dulieu O, Kosloff R and Masnou-Seeuws F 1999 *J. Chem. Phys.* **110** 9865
[42] Willner K, Dulieu O and Masnou-Seeuws F 2004 *J. Chem. Phys.* **120** 548
[43] Kosloff R 1988 *J. Phys. Chem.* **92** 2087